Pyranopterin conformation defines the function of molybdenum and tungsten enzymes

Richard A. Rothery[a], Benjamin Stein[b], Matthew Solomonson[a], Martin L. Kirk[b], and Joel H. Weiner[a,1]

[a]Department of Biochemistry, University of Alberta, Edmonton, AB, Canada T6G 2H7; and [b]Department of Chemistry and Chemical Biology, University of New Mexico, Albuquerque, NM 87131

Edited by Harry B. Gray, California Institute of Technology, Pasadena, CA, and approved August 3, 2012 (received for review January 12, 2012)

We have analyzed the conformations of 319 pyranopterins in 102 protein structures of mononuclear molybdenum and tungsten enzymes. These span a continuum between geometries anticipated for quinonoid dihydro, tetrahydro, and dihydro oxidation states. We demonstrate that pyranopterin conformation is correlated with the protein folds defining the three major mononuclear molybdenum and tungsten enzyme families, and that binding-site microtuning controls pyranopterin oxidation state. Enzymes belonging to the bacterial dimethyl sulfoxide reductase (DMSOR) family contain a metal-bis-pyranopterin cofactor, the two pyranopterins of which have distinct conformations, with one similar to the predicted tetrahydro form, and the other similar to the predicted dihydro form. Enzymes containing a single pyranopterin belong to either the xanthine dehydrogenase (XDH) or sulfite oxidase (SUOX) families, and these have pyranopterin conformations similar to those predicted for tetrahydro and dihydro forms, respectively. This work provides keen insight into the roles of pyranopterin conformation and oxidation state in catalysis, redox potential modulation of the metal site, and catalytic function.

energetics | molybdoenzymes | redox chemistry

The pyranopterin dithiolene ligand is present in all molybdenum (Mo) and tungsten (W) containing enzymes with the exception of nitrogenase (1). These enzymes, known as mononuclear Mo/W enzymes, play pivotal roles in metabolism, global geochemical cycles, and microbial metabolic diversity (2–5). Their active sites, comprising a Mo or W ion and one or two pyranopterins, catalyze a diversity of redox transformations spanning a reduction potential range of approximately one volt. While the immediate environment of the substrate-binding metal ion is critically important in catalysis (6), little attention has been focused on the impact of variations in pyranopterin structure on enzyme function.

Protein-bound pyranopterins are typically interpreted as having the tricyclic structure depicted in Fig. 1*A*, comprising pyrimidine, piperazine, and pyran-dithiolene rings. The dithiolene chelate binds a single Mo/W atom, which constitutes the catalytic active site. The pyranopterin shown in Fig. 1*A* is also known as the tetrahydro mononucleotide form due to the oxidation state of its piperazine ring and the presence of a phosphomethyl group attached to its C-2 atom (1). This form is assigned to the xanthine dehydrogenases, and in its cytosine dinucleotide form to the bacterial carbon monoxide dehydrogenases and aldehyde dehydrogenases (these enzymes are referred to collectively as the XDH family). It is also assigned to the sulfite oxidases and plant nitrate reductases [SUOX family (1, 5)].

Mononuclear Mo/W enzymes also coordinate metal-bis-pyranopterin cofactors, either as the metal-bis(pyranopterin guanine dinucleotide) form (Fig. 1*D*) found in the dimethyl sulfoxide reductase family of molybdoenzyme subunits (DMSOR family), or the mononuclear bis-pyranopterin form found in the thermophilic aldehyde oxidoreductases [AOR family (7)]. The reason for the presence of a second pyranopterin in the bis-pyranopterin-containing enzymes remains unclear. It could function to orient the metal center for optimization of substrate binding and catalysis (8), but this can also be achieved without a second pyranopterin (e.g., nitrate reductases exist in both the DMSOR and SUOX families). An attractive hypothesis is that the second pyranopterin enables additional facets of redox tuning to facilitate catalysis, thus contributing to the diversity of reactions catalyzed by these enzymes.

Dithiolenes display remarkable non-innocent behavior in small molecule analogues of pyranopterin Mo active sites (9–11). This non-innocence extends the redox cycling of the metal through its VI/V/IV oxidation states to include two electron redox reactions of the dithiolene ligand via access to the reduced ene-dithiolate, radical dithiolene, and oxidized dithione forms (12–14). Inspection of the tetrahydro pyranopterin structure reveals the potential for additional oxidation states, such as the quinonoid 4a,10a-dihydro form (Fig. 1*B*) and the 10,10a dihydro form shown in Fig. 1*C*. Studies on bicyclic pterins suggest that the direct oxidation product of tetrahydro pyranopterin is likely to be the quinonoid 4a,10a dihydro form and that this may rearrange to the more thermodynamically stable 10,10a- dihydro form (12, 13, 15–17). An additional form of the cofactor that is observed in just two enzymes is the bicyclic pyran ring-opened form (18, 19). Little attention has been focused on the role of the pyranopterin in catalysis and its ability to accommodate alternative conformations or oxidation states. In general, experimental assignment of its oxidation state is confounded by its in vitro lability: it is rapidly degraded upon release from the protein to well-characterized oxidized derivatives under laboratory conditions (13, 20). Attempts to experimentally assign oxidation state to the pyranopterins of rat liver sulfite oxidase and bovine milk xanthine oxidase yielded conflicting assignments ranging from tetrahydro to dihydro to quinonoid dihydro (21–23). Thus, the precise oxidation state of the pyranopterins within molybdoenzymes remains unresolved.

We have employed a conformational analysis approach augmented by electronic structure calculations to assess the nature of pyranopterin distortions in the mononuclear Mo/W enzymes. We find that the pyranopterin conformations in the enzymes are described by a well-defined distortion coordinate which encompasses conformations expected for quinonoid dihydro, tetrahydro, and dihydro pyranopterin oxidation states. The relationship between pyranopterin conformation and oxidation state provides the first structural evidence indicating that enzyme-bound pyranopterins can exist in both tetrahydro and dihydro forms. Furthermore, we identify a critical relationship between pyranopterin conformation and enzyme function, since specific distortions are related to the protein fold for each enzyme family (SUOX, XDH, DMSOR, AOR families). Our studies provide

Author contributions: R.A.R., M.L.K., and J.H.W. designed research; R.A.R., B.S., and M.S. performed research; R.A.R., B.S., M.S., and M.L.K. analyzed data; and R.A.R., B.S., M.L.K., and J.H.W. wrote the paper.

The authors declare no conflict of interest.

This article is a PNAS Direct Submission.

[1]To whom correspondence should be addressed. E-mail: jweiner@ualberta.ca.

This article contains supporting information online at www.pnas.org/lookup/suppl/doi:10.1073/pnas.1200671109/-/DCSupplemental.

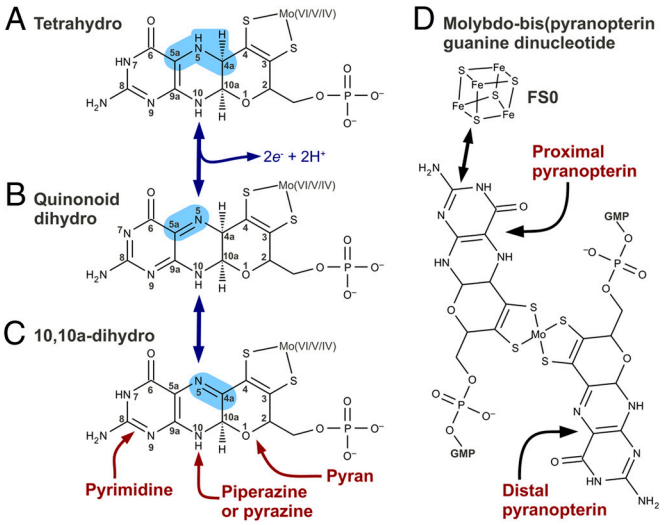

Fig. 1. Structure of the pyranopterin cofactor. Tetrahydro (*A*), quinonoid dihydro (*B*), and 10,10a-dihydro (*C*) forms are shown. Oxo groups and the protein-Mo ligand are omitted for brevity. Panel *D* shows the structure of the bis-pyranopterin cofactor (with attached GMP) that is found in the DMSO reductase (DMSOR) class enzymes. In this case, the proximal pyranopterin is closest to an [Fe-S] cluster referred to as FS0. For reasons described in the text, the proximal pyranopterin is shown in its tetrahydro form, whereas the proximal pyranopterin is shown in its dihydro form.

unique insights into the chemical reactivity and structure of the pyranopterin component of the mononuclear Mo/W cofactor.

Results and Discussion

In DMSOR family enzymes, the two pyranopterins are referred to as proximal and distal based on their proximity to an iron-sulfur cluster known as FS0* [Fig. 1*D* (1, 24)]. Fig. 2*A* shows a structural alignment of the two pyranopterins of the periplasmic nitrate reductase from *Cupriavidus necator* (a member of the DMSOR family) (25). The proximal pyranopterin (cyan) is more distorted than the distal pyranopterin (green), with the distortions being limited to the piperazine and pyran rings. Careful examination of pyranopterin structures identified two dihedral angles (defined as α and β) that allow quantification of distortions across the four families of mononuclear Mo/W enzymes. The angle α is defined by C-9a (*a*), N-10 (*b*), C-10a (*c*), and C-4a (*d*); and β is defined by *a*, *b*, *c*, and O-1 (*e*). Fig. 2*B* illustrates how the angle measurements report on the respective ring conformations. Here, a more negative α indicates a more distorted piperazine with C-4a descending below the pyrimidine-piperazine plane. A β angle of 180° is consistent with pyran-piperazine co-planarity, and a β angle of value of 90° is consistent with pyran-piperazine perpendicularity. As described below, measurement of α and β dihedrals of protein-bound and computational model pyranopterins provides new insights into pyranopterin function in the mononuclear Mo/W enzymes.

Database searches identified five members of the SUOX family, seven members of the XDH family, 15 members of the DMSOR family, and one member of the AOR family. A total of 102 protein structures were identified that possess 319 individual pyranopterins that were analyzed as described above. Table S1 summarizes the enzymes analyzed, their pyranopterin α and β angles, and provides statistics on angle variability within structures describing individual enzymes. For the purposes of our analyses, similar enzymes from different sources with different primary sequences were treated as distinct enzymes (e.g., periplasmic nitrate reductases from four sources were analyzed individually).

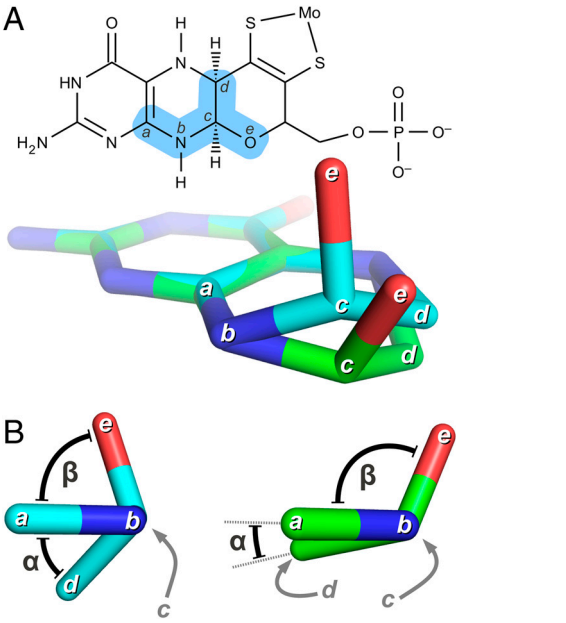

Fig. 2. Piperazine-pyran conformational analyses. (*A*) Dihedral angles α and β are defined by atoms *a-b-c-d and a-b-c-e* (as defined in the text). Proximal and distal pyranopterins of a periplasmic nitrate reductase (PDB code 3ML1), with pyran ring carbons and Mo dithiolene omitted for clarity. Carbons atoms are shown in cyan (proximal, P) and green (distal, D). (*B*) Representation of the α and β dihedral angles. The left and right images represent the proximal and distal pyranopterins, respectively. The angle α is −48.4° and −11.4°; whereas β is 70.3° and 111.9° for the proximal and distal pyranopterins, respectively.

When representative pyranopterins are aligned and their conformations compared, those of the SUOX family resemble the DMSOR distal pyranopterins, while those of the XDH family resemble the DMSOR proximal pyranopterins (Fig. 3*A*). These observations are reinforced by comparison of the measured angles and their standard deviations, indicating statistically-significant overlap between the conformations of the SUOX family pyranopterins and those of the DMSOR distal pyranopterins; as well as between the conformations of the XDH family pyranopterins and those of the DMSOR proximal pyranopterins (Fig. 3*B*).† This trend is continued in the single representative of the AOR family, in which its distal pyranopterin has a less distorted conformation than its proximal pyranopterin (Table S1). These observations demonstrate a clear correlation between protein fold and pyranopterin conformation.

Before the differences in pyranopterin conformations can be interpreted, the robustness of the crystallographic data upon which our measurements are based must be established. Fitting of the pyranopterin atoms to electron density maps has the potential to be biased by assumptions made during model building, especially at lower crystallographic resolutions. This issue was addressed in two ways: (*i*) we established that all angle measurements are unique in protein structures containing multiple pyranopterins, indicating that individual equivalent pyranopterins were treated independently during model building; and (*ii*) we evaluated the relationship between the angles measured and the reported crystallographic resolution. Fig. S3 shows plots of α and β angles as a function of crystallographic resolution for all the SUOX/XDH/DMSOR family structures containing multiple equivalent pyranopterins. There is no significant dependence of measured angles on decreasing resolution, indicating that we can

*Evolution has resulted in the loss of the FS0 cluster from some DMSOR family enzymes, but the positions of the two pyranopterins are retained within the conserved protein fold.

†See supplemental Figs. S1 and S2 for comparison of the angles of individual enzymes.

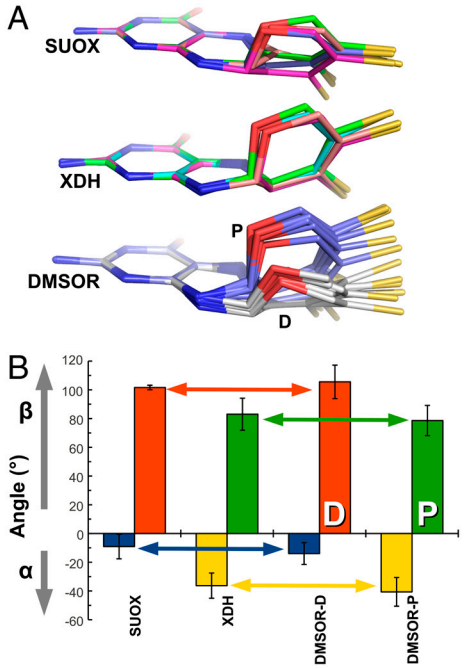

Fig. 3. Pyranopterin conformations in the SUOX, XDH, and DMSOR families. (*A*) Atoms of the pyrimidine ring were aligned and the images rendered to show differences in piperazine and pyran ring conformations. Examples of each family are shown with PDB codes in parentheses. SUOX: nitrate reductase (2BII); sulfite oxidase (1SOX); YedY (1XDQ); and sulfite dehydrogenase (2BLF). XDH: carbon monoxide dehydrogenase (1FFV and 1N62); 4hydroxybenzoyl-CoA reductase (1RM6); Quinoline-2-oxidoreductase (1T3Q). DMSOR: DMSO reductase (2DMR); arsenite oxidase (1G8K); periplasmic nitrate reductase (2V3V); periplasmic nitrate reductase (3NYA); respiratory nitrate reductase (1R27); and polysulfide reductase (2VPZ). Carbon atoms of proximal (P) and distal (D) pyranopterins are rendered in blue and grey, respectively. (*B*) Averaged angle data from the enzymes represented in Table S1 are presented with values from each enzyme having equivalent weight. In *t*-tests, the SUOX and DMSOR distal pyranopterin datasets yielded *P*-values of 0.30 and 0.22 for the α and β angles, respectively; and the XDH and DMSOR proximal pyranopterin datasets yielded *P*-values of 0.32 and 0.40, respectively. All other measured *P*-values were less than 0.004.

confidently use crystallographic data to draw the conclusions presented herein.

We hypothesize that the differences in observed conformations result from the presence of alternative redox states within Mo/W enzyme structures. For example, inspection of the structures of Fig. 1 indicates that the tetrahydro and quinonoid dihydro forms should have more distorted conformations than the 10,10a-dihydro form, which has π-delocalization extending from the pyrimidine ring to the dithiolene chelate (illustrated as a double bond between N-5 and C-4a in Fig. 1*C*). Computational models of tetrahydro, quinonoid dihydro, and 10,10a-dihydro pyranopterins demonstrate that of the available redox states and tautomers, only these fall within the conformational range defined by available protein structures. The tetrahydro, quinonoid dihydro, and 10,10a-dihydro models possess α and β angles of −38.3° and 84.8°, −50.4° and 69.5°, and −7.8° and 112.2°, respectively. Models of the alternative 5,10- and 4a,5- dihydro tautomers have β angles far outside the range described in Table S1 and Fig. 3*B*.[‡]

To correlate pyranopterin geometries with redox state, we plotted the dihedral angle β as a function of α (Fig. 4). The plot can be fitted to a linear function with good correlation (slope of 0.93, correlation coefficient of 0.87) and represents a distortion coordinate of available conformations. Pyranopterins falling on the upper right of the plot are more planar, while those falling on the lower left are more distorted. Critically, the data points corresponding to the computed tetrahydro, quinonoid dihydro, and 10,10a-dihydro forms fall close to the linear fit to the experimental data. The computed quinonoid dihydro form roughly defines one extreme of the plot of Fig. 4, with only two experimentally observed pyranopterins being significantly more distorted (the proximal pyranopterins from *E. coli* nitrate reductase and *Aromatoleum aromaticum* ethylbenzene dehydrogenase, NARG_ECOLI and Q5P5I0_AROAE). The computed tetrahydro and 10,10a-dihydro forms fall within the distributions of the DMSOR proximal and distal pyranopterins, respectively, and the distribution of XDH pyranopterins is similar to that of the DMSOR proximal pyranopterins. In the case of the SUOX enzymes (e.g., NIA_PICAN), the data points fall towards the more planar end of the continuum, but conformational variability is largely confined to the α dihedral. These analyses suggest that pyranopterins exhibit a "redox continuum" of conformations that range from those similar to the quinonoid dihydro, tetrahydro, and 10,10a-dihydro forms along the distortion coordinate, with the tetrahydro and 10,10a-dihydro forms being representative of the majority of experimentally-determined conformations.

To further assess the influence of pyranopterin conformation on predicted oxidation state, we evaluated the relative energies of the tetrahydro, quinonoid, and 10,10a-dihydro forms in their energy minimized conformations. We then evaluated the energetics of distorting these forms into conformations corresponding to the available alternate redox states (Fig. 5*A*). Because experimental data are lacking on the energetics of the dihydro to tetrahydro pyranopterin reduction, we used the ΔG value of 28.6 kJ mol^{-1} ($E_0{}' = 0.15$ V) determined for tetrahydropterin, 6-methyltetrahydropterin, and 6,7-dimethyltetrahyropterin reduction to their respective quinonoid dihydro forms (26). The methylated 6- and 7- tetrahydropterin atoms correspond to C-4a and C-10a in the structures presented in Fig. 1. With this caveat, we note that in our analyses the two lowest energy pyranopterins are the tetrahydro and 10,10a-dihydro forms. Each of the available distortions presented in Fig. 5*A* increases the free energy of

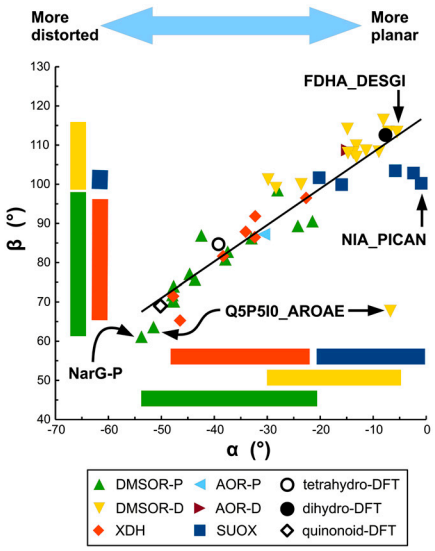

Fig. 4. A distortion coordinate describing pyranopterin conformations. Angle β was plotted vs angle α. Each data point corresponds to average values for the individual enzymes. Data points corresponding to models of the tetrahydro, quinonoid, and dihydro pyranopterins are also shown, as are points corresponding the the aldehyde oxidoreductase from *Pyrococcus furiosus* (AOR-P and AOR-D). The outlier Q5P5I0_AROAE is not included in the linear regression fit. The slope of the line is 0.93 ± 0.06, with an correlation coefficient of 0.87. Colored bars represent the range of the measurements for the individual enzyme families (color-coded to match the data points).

[‡]Angles for the alternate tautomers were: 5,10-dhiydro, α = 0.5° and β = 174°; 4a,5-dihydro, α = −5° and β = 175.5°.

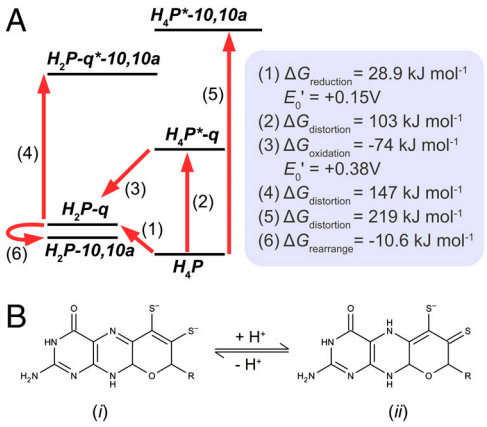

Fig. 5. (*A*) Energetics of pyranopterin distortion and oxidation. H_4P, energy minimized tetrahydro pyranopterin; H_2P-q, energy minimized quinonoid dihydro; H_2P-10,10a, energy minimized 10,10a-dihydro; H_4P^*-q, tetrahydro at quinonoid dihydro geometry; H_4P^*-10,10a, tetrahydro at 10,10a-dihydro geometry; H_2P-q*-10,10a, quinonoid dihydro at 10,10a-dihydro geometry. We note that calculation of tautomer energy differences can be sensitive to the choice of method and/or basis set. (*B*) (*i*) Dihydro pyranopterin possessing a dianionic dithiol chelate. (*ii*) Protonated form of the dihydro pyranopterin possessing a monoanionic thiol/thione type dithiolene chelate.

the system to an extent much greater than the equivalent available redox reaction. Distortion of the tetrahydro form to the 10,10a-dihydro conformation occurs at the expense of 219 kJ mol^{-1}, whereas the corresponding oxidation to the dihydro quinonoid form expends an estimated 28.9 kJ mol^{-1} (26). In the bicyclic pterins, the quinonoid oxidation product is predicted to rearrange to the 6,7-dihydro form structurally equivalent to the 10,10a-dihydro pyranopterin (13, 16). The conformational destabilizations summarized in Fig. 5*A* provide strong driving forces for the corresponding available redox reactions, suggesting it is unlikely that the continuum of pyranopterin distortions depicted in Fig. 4 arises solely from a single oxidation state. This supports our hypothesis that oxidation state and electronic structure can be influenced by conformational distortions.

Comparison of Fig. 1*C* with Fig. 1*A* reveals that a more extensive pyranopterin π-delocalization exists in the 10,10a-dihydro form than in the tetrahydro form. This facilitates electronic communication between the dithiolene chelate and the pyrimidine ring of the dihydro form, decreasing the electron donating ability of the dithiolene to the Mo/W ion. Thus, a dihydro pyranopterin dithiolene chelate should result in more positive Mo/W(V/IV) and Mo/W(VI/V) reduction potentials than those of a tetrahydro pyranopterin dithiolene chelate. Inspection of the dihydro pyranopterin structure reveals an additional mechanism by which modulation of the Mo/W reduction potentials can occur. Protonation of N-5 can facilitate an internal redox reaction between the piperazine ring and the dithiolene (27, 28), leading to the formation of a monoanionic thiol-thione type chelate (Fig. 5*B*). In support of this, a monoanionic, thiol-thione type dithiolene was recently observed in a Mo-dithiolene model complex that possesses a donor-acceptor dithiolene ligand bound to a reduced Mo(IV) ion (14). The accessibility of a thiol-thione dihydro pyranopterin chelate (Fig. 5*B*) impacts two critical features of the Mo/W enzymes to which it is accessible: (*i*) By formally decreasing the dithiolene net charge from −2 to −1, it should shift the Mo/W reduction potentials to markedly more positive values; and (*ii*) selective stabilization of a thione sulfur attached to C-3 may play a critical role in defining the geometry and reactivity of the Mo/W coordination sphere via a trans effect/influence. This may be critical in explaining the differences in coordination sphere geometries and reactivities observed in the XDH and SUOX enzyme families (29).

Each data point in the plot of Fig. 4 represents an individual enzyme as listed in Table S1. It is notable that there is overlap in the reported ranges for the α angles for the proximal and distal pyranopterins of the DMSOR family, but not between such angles of the SUOX and XDH families. In the individual DMSOR family enzymes, the proximal pyranopterin always has a more distorted conformation than the distal pyranopterin. The most extreme outlier in Fig. 4 corresponds to the distal pyranopterin of the *Aromatoleum aromaticum* ethylbenzene dehydrogenase [Q5P5I0_AROAE (18)]. In this case, the pyranopterin is bicyclic, with the pyran oxygen being held in a distorted position relative to what would be the pyranopterin C-10a position by an Arg side chain guanidinium.

Our data support the hypothesis that in the majority of Mo/W enzymes, binding site micro-tuning favors either the dihydro or tetrahydro oxidation state. A critical question is whether existing experimental data can be interpreted in the context of these states being accessible in vivo. Protein film voltammetry (PFV) (30) has been used to evaluate the potential-dependent activity of a range of molybdoenzymes. In DMSOR family members that are reductases, enzyme activity increases with increasing driving force (decreasing electrode potential) until a specific potential is reached, beyond which enzyme activity is attenuated. This phenomenon is described by a reduction potential referred to as E_{switch}. It has been suggested (31) that this behavior is simply a reflection of enzyme activity being optimal at potentials where the Mo(V) redox intermediate is more prevalent. However, there is a lack of correlation within the DMSOR family between measured Mo reduction potentials and reported E_{switch} values, suggesting the possibility that E_{switch} arises from pyranopterin dihydro to tetrahydro reduction should be further investigated. A second line of experimental evidence arises from the application of Resonance Raman spectroscopy, which demonstrates that the two pyranopterins of the *R. sphaeroides* dimethyl sulfoxide reductase and *E. coli* biotin sulfoxide reductase are not equivalent, with vibrational modes assigned to two dithiolene-metal units, one of which has a higher C═C double bond character (32, 33), rendering it similar to the single dithiolene-metal vibrational mode observed in human sulfite oxidase (34). Although these observations may simply reflect differences in the Mo-dithiolene bonding and ligand geometry (8), they are consistent with the presence of non-equivalent proximal and distal pyranopterins, with a facet of this being differential accessibility to the tetrahydro and dihydro redox states.

The presence of a tetrahydro proximal pyranopterin and a dihydro distal pyranopterin in the DMSOR family should be reflected in differences in hydrogen bonding to the respective piperazine rings. In the tetrahydro form, N-5 and N-10 should be able to act as H-bonding donors with the nitrogen lone pair presenting the possibility of them also being H-bond acceptors. In the 10,10a-dihydro pyranopterins, N-5 should only be able to act as an H-binding acceptor, with N-10 retaining its donor functionality. Scrutiny of available structures reveals that this is indeed the case. Fig. 6*A* shows the structure surrounding the bis-pyranopterin from a periplasmic nitrate reductase (PDB code 2V3V), revealing possible H-bonding contacts between the protein and the N-5 and N-10 of each pyranopterin. Two residues are shown interacting with the N-5 atom of the proximal pyranopterin, and the ND atom of His623 is shown acting as an H-bond acceptor from the proximal N-5. A second residue, Arg617, acts as a donor to N-5 via its NH1 atom. These two interactions are predicted to stabilize the sp^3 hybridization and a more tetrahedral geometry of the proximal N-5, consistent with the proximal pyranopterin being in the tetrahydro form (and inconsistent with it being in the dihydro quinonoid form). This contrasts with the H-bonding environment of the distal N-5. In this case there is a single plausible donor (the NH2 atom of Arg617), but no plausible acceptor. In both cases the N-10 atom appears to function as an H-bond donor to backbone amide oxygens (Ala180 and

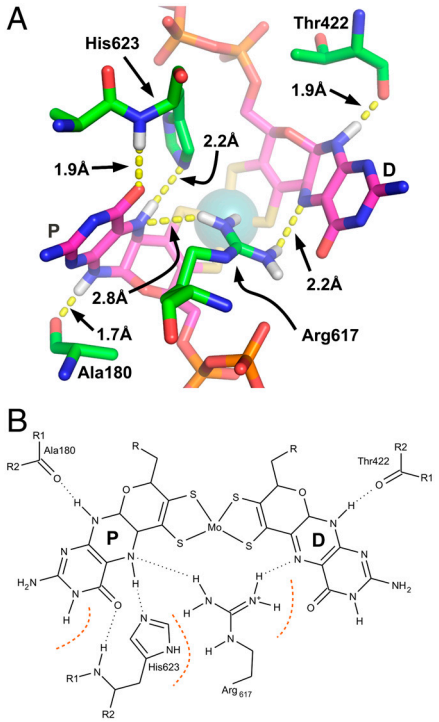

Fig. 6. (*A*) Residues coordinating the pyranopterin piperazine ring in the periplasmic nitrate reductases. The figure shows the structure of the periplasmic nitrate reductase from *Desulfovibrio desulfuricans* (PDB code 2V3V), and is also representative of those from *Rhodobacter sphaeroides* (PDB code 1OGY) and *Cupriavidus necator* (PDB code 3ML1). (*B*) Proposed H-bonding network around the piperazine rings of the proximal and distal pyranopterins. The proximal pyranopterin is shown in its tetrahydro form, with this oxidation state stabilized by both the conserved bridging Arg and the conserved redox-state stabilizing His. The distal pyranopterin is shown in its dihydro form with the N-5 atom being an H-bonding acceptor from the guanidinium group of Arg617.

Thr422, respectively). Fig. 6*B* summarizes piperazine nitrogen H-bond interactions, and represents a conserved theme across the entire DMSOR family. In every case there is a residue, either an Arg or a His that bridges the proximal and distal piperazines, and in almost every case (14 out of 15 enzymes) there is second residue, typically a His, Gln, or Ser that H-bonds to the proximal N-5, favoring a tetrahedral geometry for this atom (Table S2). The proximal pyranopterin N-10 atom appears to function as an H-bonding donor in every case analyzed to a backbone amide oxygen. In 14 out of 15 enzymes analyzed, the distal pyranopterin N-10 also appears to be an H-bond donor to a backbone amide oxygen. These analyses support the concept of binding site microtuning to favor a tetrahydro oxidation state for the proximal pyranopterin and a dihydro oxidation state for the distal pyranopterin in the DMSOR family. Analyses of pyranopterin contact residues in the SUOX and XDH families do not provide such clear insights into possible oxidation states.

Our analyses reveal an emerging correlation between pyranopterin conformation and potential function in electron-transfer to and from the catalytically critical Mo/W atom (Fig. S4). In the SUOX family, electron transfer between the Mo and the heme does not occur along a vector close to the pyranopterin, rendering it an unlikely direct participant (35, 36). In the XDH family, an electron transfer relay consisting of two [2Fe-2S] clusters connects the pyranopterin to an FAD binding site where the second substrate of the enzyme binds, typically NAD^+ (37), rendering electron transfer through the pyranopterin plausible. In the DMSOR and AOR families, electron transfer is plausible to/from the Mo/W atom through the proximal pyranopterin, but not through the distal pyranopterin. Our results suggest that pyranopterins implicated as electron-transfer conduits have conformations consistent with a tetrahydro oxidation state, whereas those not implicated as such have conformations consistent with a dihydro oxidation state. Given that oxidation of the tetrahydro form to the dihydro form should have a profound effect on Mo/W redox chemistry, we propose that the binding sites of the XDH and DMSOR proximal pyranopterins evolved to prevent inadvertent oxidation of the pyranopterin that could negatively impact catalysis.

Prior insights on the oxidation states available to the pyranopterin ring system have come from studies of bicyclic pterin models and tricyclic models such as pyranoneopterin (12, 13, 15). These showed that in model compounds oxidation of pyranopterin is always accompanied by pyran ring opening and that the pyran ring blocks formation of the 10,10a-dihydro form. However, our structural analyses suggest that the tricyclic 10,10a-dihydro form may be present in some DMSOR and SUOX enzymes. This is the first evidence suggesting a biological role for the tricyclic dihydro pyranopterin. We stress that the assignment of the DMSOR proximal and distal pyranopterins to tetrahydro and dihydro oxidation states does not imply obligatory redox cycling during catalysis. This, along with metal chelation, marks an important distinction between pterin-containing enzymes such as phenylalanine hydroxylase and the pyranopterin-containing Mo/W enzymes described herein. Our analyses support the hypothesis that a synergistic interaction exists between pyranopterin redox state and binding site conformational and hydrogen-bonding constraints mediated by the protein. These factors create unique opportunities for using pyranopterin tautomers that are both distinct from and have distinct functions from those used in other pterin containing enzyme systems.

We have demonstrated that protein-bound pyranopterins adopt a continuum of conformations which can be described by a well-defined distortion coordinate. Energetic analyses of computed structures demonstrate that this coordinate likely joins in-protein tetrahydro and dihydro oxidation states, with the possibility that the most distorted pyranopterins may be in the quinonoid dihydro form. Our observations provide new insights into how pyranopterin redox flexibility can be harnessed to tune metal center redox chemistry and electron transfer within the mononuclear Mo/W enzyme families. In the bis-pyranopterin containing enzymes, this provides for maximum flexibility in active site redox tuning, allowing one pyranopterin to be involved in vectorial electron-transfer with endogenous and exogenous redox partners, and a second pyranopterin to assist in redox tuning of the active site.

Materials and Methods

Identification of Mononuclear Mo/W Enzymes. The structural dataset used in our analyses was obtained by searching the PDB database with the PDBeFold server (38). Individual structures are identified by their PDB codes in the *SI Text*.

Dihedral Angle Measurements. Individual pyranopterins were identified in protein structures, and dihedral angles were measured using the MarvinSpace application (www.chemaxon.com). The atoms defining the dihedrals are described in the text.

DFT Calculations. Gas phase DFT calculations were performed with ADF 2010.01 (Scientific Computing and Modeling, www.scm.com) using the PBE GGA functional and the DZP basis set. All quoted DFT angles are for non-metallated pyranopterins; calculations with metallated pyranopterins only show a slight deviation in angles (1–5°).

ACKNOWLEDGMENTS. We thank Sharon Burgmayer for insights into pyranopterin chemistry and Justin Fedor for critical reading of the manuscript. This work was funded in part by the Canadian Institutes of Health Research (Grant MOP106550 to J.H.W.), and by the US National Institutes of Health (Grant GM-057378 to M.L.K.).

1. Magalon A, Fedor JG, Walburger A, Weiner JH (2011) Molybdenum enzymes in bacteria and their maturation. *Coord Chem Rev* 255:1159–1178.
2. Romao MJ (2009) Molybdenum and tungsten enzymes: A crystallographic and mechanistic overview. *Dalton Trans* 4053–4068.
3. Hille R (2002) Molybdenum enzymes containing the pyranopterin cofactor: An overview. *Met Ions Biol Syst* 39:187–226.
4. Schwarz G, Mendel RR, Ribbe MW (2009) Molybdenum cofactors, enzymes and pathways. *Nature* 460:839–847.
5. Workun GJ, Moquin K, Rothery RA, Weiner JH (2008) Evolutionary persistence of the molybdopyranopterin-containing sulfite oxidase protein fold. *Microbiol Mol Biol Rev* 72:228–248.
6. Pushie MJ, George GN (2011) Spectroscopic studies of molybdenum and tungsten enzymes. *Coord Chem Rev* 255:1055–1084.
7. Chan MK, Mukund S, Kletzin A, Adams MW, Rees DC (1995) Structure of a hyperthermophilic tungstopterin enzyme, aldehyde ferredoxin oxidoreductase. *Science* 267:1463–1469.
8. Mtei RP, et al. (2011) Spectroscopic and electronic structure studies of a dimethyl sulfoxide reductase catalytic intermediate: Implications for electron- and atom-transfer reactivity. *J Am Chem Soc* 133:9762–9774.
9. Matz KG, Mtei RP, Leung B, Burgmayer SJN, Kirk ML (2010) Noninnocent dithiolene ligands: A new oxomolybdenum complex possessing a donor–acceptor dithiolene ligand. *J Am Chem Soc* 132:7830–7831.
10. Helton ME, et al. (2001) Thermally driven intramolecular charge transfer in an oxo-molybdenum dithiolate complex. *J Am Chem Soc* 123:10389–10390.
11. Mtei RP, et al. (2011) A valence bond description of dizwitterionic dithiolene character in an oxomolybdenum-bis(dithione) complex. *Eur J Inorg Chem*, in press.
12. Nieter Burgmayer SJ, Pearsall DL, Blaney SM, Moore EM, Sauk-Schubert C (2004) Redox reactions of the pyranopterin system of the molybdenum cofactor. *J Biol Inorg Chem* 9:59–66.
13. Basu P, Burgmayer SJN (2011) Pterin chemistry and its relationship to the molybdenum cofactor. *Coord Chem Rev* 255:1016–1038.
14. Matz KG, Mtei RP, Rothstein R, Kirk ML, Burgmayer SJN (2011) Study of molybdenum(4+) quinoxalyldithiolenes as models for the noninnocent pyranopterin in the molybdenum cofactor. *Inorg Chem* 50:9804–9815.
15. Enemark JH, Garner CD (1997) The coordination chemistry and function of the molybdenum centres of the oxomolybdoenzymes. *J Biol Inorg Chem* 2:817–822.
16. Greatbanks SP, Hillier IH, Garner CD, Joule JA (1997) The relative stabilities of dihydropterins; a comment on the structureof Moco, the cofactor of the oxomolybdoenzymes. *J Chem Soc Perkin Trans* 2:1529–1534.
17. Armarego WLF, Waring P (1982) Pterins. Part 9. The structure of quinonoid dihydropterins [2-amino-7,8-dihydropteridin-4(6H)-ones]. *J Chem Soc Perkin Trans* 2:1227–1233.
18. Kloer DP, Hagel C, Heider J, Schulz GE (2006) Crystal structure of ethylbenzene dehydrogenase from Aromatoleum aromaticum. *Structure* 14:1377–1388.
19. Bertero MG, et al. (2003) Insights into the respiratory electron transfer pathway from the structure of nitrate reductase A. *Nat Struct Biol* 10:681–687.
20. Hille R (1996) The mononuclear molybdenum enzymes. *Chem Rev* 96:2757–2816.
21. Gardlik S, Rajagopalan KV (1990) The state of reduction of molybdopterin in xanthine oxidase and sulfite oxidase. *J Biol Chem* 265:13047–13054.
22. Gardlik S, Rajagopalan KV (1991) Oxidation of molybdopterin in sulfite oxidase by ferricyanide effect on electron transfer activities. *J Biol Chem* 266:4889–4895.
23. Rajagopalan KV, Kramer S, Gardlik S (1986) Studies on the oxidation state of molybdopterin. *Polyhedron* 5:573–576.
24. Rothery RA, Workun GJ, Weiner JH (2008) The prokaryotic complex iron-sulfur molybdoenzyme family. *Biochim Biophys Acta* 1778:1897–1929.
25. Coelho C, et al. (2011) The crystal structure of Cupriavidus necator nitrate reductase in oxidized and partially reduced states. *J Mol Biol* 408:932–948.
26. Archer MC, Scrimgeour KG (1970) Reduction potentials of tetrahydropterins. *Can J Biochem* 48:526–527.
27. Pan WH, Harmer MA, Halbert TR, Stiefel EI (1984) Induced internal redox processes in molybdenum-sulfur chemistry: Conversion of tetrathiomolybdate(2-) ion to octathiodimolybdate(2-) ion by organic disulfides. *J Am Chem Soc* 106:459–460.
28. David Garner C, et al. (1993) Synthesis of cyclopentadiemnyk-ene-1,2-dithiolatocobalt complexes and coupled proton-electron transfer in a substituted quinaxalinyl derivatives. *Heterocycles* 35:563–568.
29. Schwarz G, Mendel RR (2006) Molybdenum cofactor biosynthesis and molybdenum enzymes. *Annu Rev Plant Biol* 57:623–647.
30. Armstrong FA (2005) Recent developments in dynamic electrochemical studies of adsorbed enzymes and their active sites. *Curr Opin Chem Biol* 9:110–117.
31. Heffron K, Léger C, Rothery RA, Weiner JH, Armstrong FA (2001) Determination of an optimal potential window for catalysis by E. coli dimethyl sulfoxide reductase and hypothesis on the role of Mo(V) in the reaction pathway. *Biochemistry* 40:3117–3126.
32. Garton SD, et al. (1997) Active site structures and catalytic mechanism of Rhodobacter sphaeroides dimethyl sulfoxide reductase as revealed by Resonance Raman spectroscopy. *J Am Chem Soc* 119:12906–12916.
33. Garton SD, et al. (2000) Resonance Raman characterization of biotin sulfoxide reductase Comparing oxomolybdenum enzymes in the ME(2)SO reductase family. *J Biol Chem* 275:6798–6805.
34. Garton SD, Garrett RM, Rajagopalan KV, Johnson MK (1997) Resonance Raman characterization of the molybdenum center in sulfite oxidase: Identification of MoO stretching modes. *J Am Chem Soc* 119:2590–2591.
35. Utesch T, Mroginski MA (2010) Three-dimensional structural model of chicken liver sulfite oxidase in its activated form. *J Phys Chem Lett* 1:2159–2164.
36. Pushie MJ, George GN (2010) Active-site dynamics and large-scale domain motions of sulfite oxidase: A molecular dynamics study. *J Phys Chem B* 114:3266–3275.
37. Holger D (2011) Structural aspects of mononuclear Mo/W-enzymes. *Coord Chem Rev* 255:1104–1116.
38. Krissinel E, Henrick K (2004) Secondary-structure matching (SSM), a new tool for fast protein structure alignment in three dimensions. *Acta Crystallogr D Biol Crystallogr* 60:2256–2268.